

Enhancement of sensitivity and bandwidth of gravitational wave detectors using fast-light-based white light cavities

This article has been downloaded from IOPscience. Please scroll down to see the full text article.

2010 J. Opt. 12 104014

(<http://iopscience.iop.org/2040-8986/12/10/104014>)

View [the table of contents for this issue](#), or go to the [journal homepage](#) for more

Download details:

IP Address: 129.105.6.42

The article was downloaded on 08/11/2011 at 00:19

Please note that [terms and conditions apply](#).

Enhancement of sensitivity and bandwidth of gravitational wave detectors using fast-light-based white light cavities

M Salit^{1,3} and M S Shahriar^{1,2}

¹ Department of Physics and Astronomy, Northwestern University, 2145 Sheridan Road, Evanston, IL 60208, USA

² Department of Electrical Engineering and Computer Science, Northwestern University, 2145 Sheridan Road, Evanston, IL 60208, USA

E-mail: m-salit@u.northwestern.edu

Received 16 March 2010, accepted for publication 21 June 2010

Published 24 September 2010

Online at stacks.iop.org/JOpt/12/104014

Abstract

The effect of gravitational waves (GWs) has been observed indirectly, by monitoring the change in the orbital frequency of neutron stars in a binary system as they lose energy via gravitational radiation. However, GWs have not yet been observed directly. The initial LIGO apparatus has not yet observed GWs. The advanced LIGO (AdLIGO) will use a combination of improved techniques in order to increase the sensitivity. Along with power recycling and a higher power laser source, the AdLIGO will employ signal recycling (SR). While SR would increase sensitivity, it would also reduce the bandwidth significantly. Previously, we and others have investigated, theoretically and experimentally, the feasibility of using a fast-light-based white light cavity (WLC) to circumvent this constraint. However, in the previous work, it was not clear how one would incorporate the white light cavity effect. Here, we first develop a general model for Michelson-interferometer-based GW detectors that can be easily adapted to include the effects of incorporating a WLC into the design. We then describe a concrete design of a WLC constructed as a compound mirror, to replace the signal recycling mirror. This design is simple, robust, completely non-invasive, and can be added to the AdLIGO system without changing any other optical elements. We show a choice of parameters for which the signal sensitivity as well as the bandwidth are enhanced significantly over what is planned for the AdLIGO, covering the entire spectrum of interest for gravitational waves.

Keywords: gravitational wave detection, fast light, white light cavity

1. Introduction

Astronomers and optical scientists have often worked together to do astronomy, and gravitational wave (GW) astronomy will not be an exception. GW detectors are not optical devices in the sense that telescopes are, but the most promising of them use interferometers to sense gravitational radiation by virtue of its effect on laser light here on Earth [1]. Here we deal with the optics of laser interferometric GW detectors. We analyze the frequency response and sensitivity for several potential designs, including a proposed modification that uses

a fast-light-based white light cavity (WLC) to enhance the sensitivity–bandwidth product. We previously demonstrated a WLC experimentally in rubidium [2], and have also explored photorefractive crystals as a potential medium for adapting the technique for use at the working wavelength of LIGO [3, 4]. We review the theory of the WLC and show mathematically the advantages it can offer for LIGO-type GW detectors.

When light travels through a region of space over which a GW is also propagating, the latter causes a periodic variation in the phase of the light field [5]. Mathematically, light with this kind of phase modulation may be described as a sum of plane waves of different frequencies. The largest frequency component is the carrier, which is just the frequency of the

³ Author to whom any correspondence should be addressed.

light when the modulation amplitude is set to zero. The next largest are the two first-order sidebands: a plus-sideband at the carrier plus the modulation frequency and a minus-sideband at the carrier minus the modulation frequency [6]. Higher-order sideband frequencies exist; however, when the modulation is small, as in the case of GWs, their amplitudes are negligible. The problem of detecting GWs may be reduced to the problem of detecting these sideband frequencies.

The difficulty lies in the fact that the amplitudes of these sideband frequency components are very small, and that they are expected to be separated generally by less than a few kilohertz, and in some cases by only tens or hundreds of hertz, from the carrier frequency. These sidebands, then, cannot be separated out from the carrier by means of the usual techniques for filtering light. Prisms and diffraction gratings will not resolve such tiny frequency differences, and even Fabry–Perot cavity filters are less than ideal for this purpose, as they would have to have linewidths down to tens of hertz and very high transmittivity on resonance, so as not to further attenuate the already weak sidebands.

Fortunately we can take advantage of a very convenient property of gravitational radiation: the fact that the modulations it causes along one axis are exactly out of phase with the modulations along a perpendicular axis [7]. We can therefore use an interferometer to separate out the carrier and the sidebands. Both Michelson and Sagnac interferometers have been proposed for this purpose. We discuss the Sagnac case in [8]. Here, we will discuss GW detectors that are variations on the Michelson interferometer.

If we arrange the arms of the interferometer along the x and y axes, and the path lengths are chosen correctly, then at one port the carrier light from the x axis will exactly cancel the carrier light from the y axis so that we get no carrier frequency light out. The interferometer is on a dark fringe for the carrier. The sidebands, however, having been created by phase modulations with opposite signs, will interfere constructively at this same port [6]. This means that we can have only the sideband light exiting one port of a Michelson interferometer under the dark fringe condition. Detecting light at that port, in theory, indicates the presence of a GW.

In practice the situation is more complicated. Most of the time light at this dark port only indicates vibrations in the interferometer mirrors or other sources of noise. A great deal of work has been done to minimize noise and to lock the interferometer on a dark fringe condition [6], but we would also like to maximize the amplitude of the sideband light falling on the detector. One way of doing that, due to the nature of GWs, is to make the arms of the interferometer very long [1].

Another approach involves the use of optical cavities within the interferometer. If the resonance linewidth of the cavities used is too small, however, then our attempts to use them to enhance the sensitivity of the GW detector will also entail narrowing its linewidth. For this reason, the ideal detector may use a white light cavity (WLC), to get the benefits of cavity enhancement described below, without correspondingly narrowing the linewidth of the detector. A WLC is a cavity that resonates over a broader range of frequencies than what its length and finesse would ordinarily

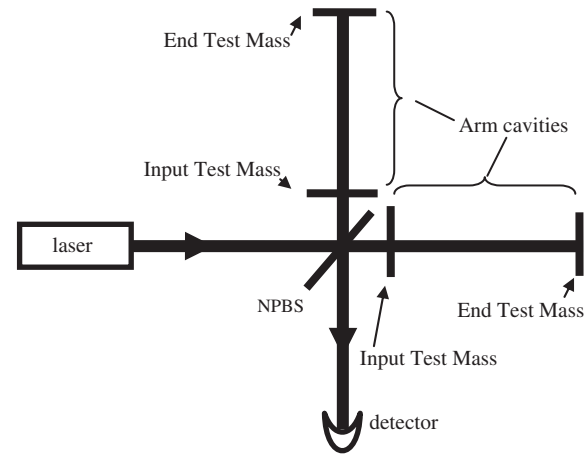


Figure 1. Michelson interferometer with arm cavities.

entail. The basic theory behind the WLC employing fast-light is discussed in section 4 below, and explored in greater detail in [9–14]. An alternative approach for realizing a WLC with a grating was first proposed in [15], but was later proved to be wrong [16].

The remainder of this paper is organized as follows. Section 2 discusses several GW detector designs that have been proposed, starting from the basic Michelson interferometer configuration. Section 3 gives a general derivation of the frequency response of devices of this type, including those described in the preceding section. Section 4 discusses the effect of a dispersive medium on that frequency response and, in particular, the effect incorporating WLCs into the design. We conclude in section 5 with a summary of our results.

2. Variations on the Michelson interferometer

There are a variety of ways to use cavities to improve the response of the Michelson-interferometer-based GW detector. One of the simplest is to add additional mirrors in each arm of the interferometer so as to turn each arm into a Fabry–Perot cavity, as illustrated in figure 1.

Sideband light is produced from the carrier on each pass as it bounces around the arm cavities. However, though the effect is similar to the use of longer cavity arms, we cannot simply model this as a system with longer effective lengths for the arms. We must take into account the interference effects of multiple bounces within these arm cavities.

We might choose to make the arm cavities resonant for the carrier frequency, for instance. This would allow us to increase the amplitude of the carrier frequency field in the arms by a potentially large factor. Since the sideband field is proportional to the carrier field, the amount of sideband light produced in the arms would then be increased by this same factor. However, the sideband light itself would also undergo multiple reflections within the arm cavities. If the frequency separation between one of the sidebands and the carrier were greater than the resonance linewidth of the cavity, then the multiple reflections of this sideband would interfere destructively. The same conclusion would apply to the other sideband as well, and

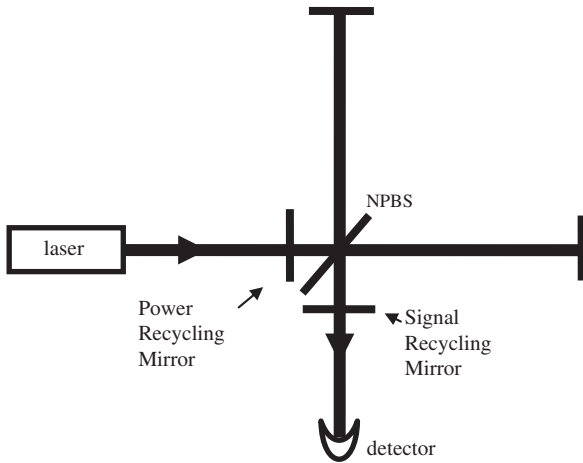


Figure 2. Michelson interferometer with dual recycling.

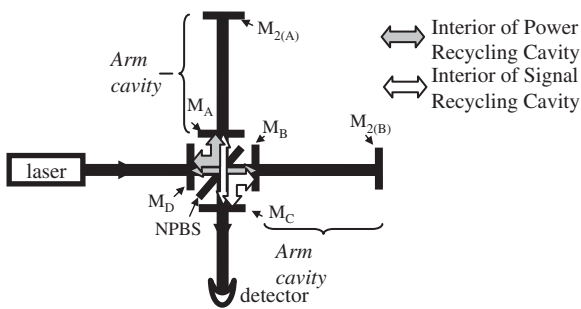


Figure 3. Michelson interferometer with dual recycling and arm cavities.

the signal at the output would be small. Similarly, we might tune the arm cavities to resonate the sidebands, but the carrier would then interfere destructively inside the cavities, making the net signal small.

One way to avoid this trade-off is to place the cavity input mirrors outside the arms of the interferometer, as illustrated in figure 2.

In this configuration, assuming the interferometer is held on the dark fringe condition, the carrier light will only be incident on the mirror labeled power recycling mirror (PRM). It will undergo multiple reflections inside both arms, as if there had been an input mirror in each. Similarly, the sideband frequency light will be reflected back into the arms by the signal recycling mirror (SRM). This dual recycling arrangement allows both the carrier and one or both of the sidebands to resonate, within separate but overlapping optical cavities. The disadvantage of this scheme is that the beamsplitter is inside the optical cavity in which the carrier resonates. The current design for advanced LIGO proposes a circulating power in the arms of 800 kW [17]. This amount of power causes thermal distortion and noise on the beamsplitter.

A third option is to combine these two designs, as illustrated in figure 3.

This system, though it comprises many overlapping compound cavities, is not much more difficult to analyze than the simpler version from figure 1, under certain conditions. If the two arm cavities are completely identical, with the

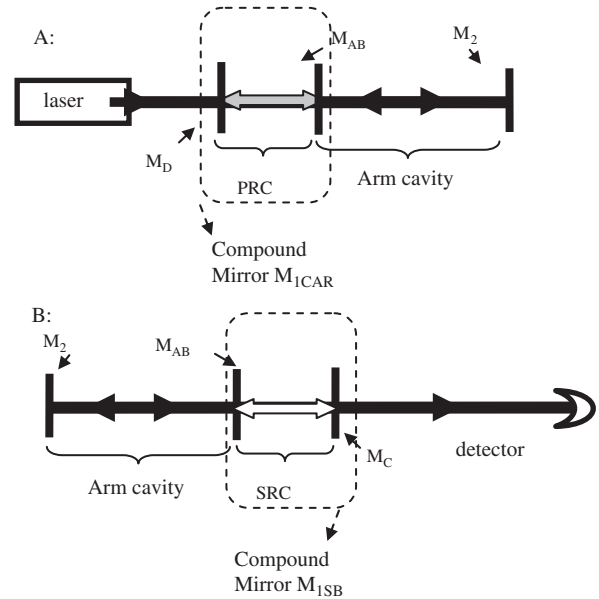


Figure 4. (A) Effective path for carrier through a system illustrated in figure 3. (B) Effective path for GW sideband through a system illustrated in figure 3.

reflectivity and position relative to the beamsplitter for the mirrors M_A and $M_{2(A)}$ being exactly the same as those for mirrors M_B and $M_{2(B)}$, then we may cease to distinguish between the end test masses $M_{2(A)}$ and $M_{2(B)}$, and refer simply to M_2 .

Likewise, since we have assumed M_A and M_B are identical, we might simply refer to M_{AB} to indicate either one of these input test mass mirrors. Carrier light that is incident on either one from the arms will then travel toward M_D , so long as the interferometer is locked on a dark fringe. Having reflected off M_D it will then travel back to one of the mirrors M_{AB} , and then back toward M_D again, so that a cavity is formed. We will refer to this cavity as the power recycling cavity (PRC).

The sideband light, likewise, travels from M_{AB} to M_C and back again, so that the sidebands experience a different cavity than the carrier. We will refer to this cavity as the signal recycling cavity (SRC).

In general, any Fabry–Perot cavity may be treated, from the outside, as a mirror that has a frequency-dependent reflectivity. Therefore, we treat the PRC, comprising M_{AB} and M_D , as a single compound mirror M_{1CAR} , because it is the compound mirror which reflects the carrier back into the arms. Likewise, we treat the SRC, comprising M_{AB} and M_C , as a single compound mirror M_{1SB} , because it is the compound mirror which reflects the sidebands back into the arms.

The total system may then be modeled as a single Fabry–Perot cavity, with one mirror M_2 having a reflectivity equal to that of the end test masses M_{2A} and M_{2B} , and one mirror M_1 , whose reflectivity is frequency-dependent, equal to that of the compound mirror M_{1CAR} for carrier frequency light, and equal to that of the compound mirror M_{1SB} for sideband frequency light. The length of this effective cavity is equal to the distance between M_A and M_{2A} (or, equivalently, between M_B and M_{2B}). This model is illustrated in figure 4.

We can now choose the length of the arm cavities to resonate one of the sidebands, the carrier, or both. However, we have the choice, thanks to the fact that we now have tunable compound mirrors, to make the finesse different for the sidebands than for the carrier. The next section analyzes the behavior of this system in mathematical detail. In this section, however, we first summarize the results qualitatively.

There are two different modes of operation for this device [18]. In both, we choose the reflectivity of M_{ICAR} to be high (by tuning the PRC length and making the reflectivity of M_D high) and choose the length of the arms so that the carrier is resonant in the arm cavities. Since the sidebands necessarily have different wavelengths from the carrier, they will be off-resonant in the arm cavities. Therefore, if we do not want the output signal to be nullified by the destructive interference of the sideband light in the arms, we must either lower the reflectivity of the compound output coupler M_{ISB} (by tuning the SRC), thus broadening the arm cavity linewidth enough to allow the sidebands to survive, or try to tune the phase the light picks up on reflection from this compound mirror to bring the sideband light back to resonance in the arms.

The idea of lowering the finesse of the arm cavities for the sidebands by using a near-resonant cavity as an output coupler is called *resonant sideband extraction* (RSE) [19]. The SRC is much shorter than the arm cavities, of the order of 50 m [20] as opposed to 4000 m, and has a correspondingly broader linewidth—at least 30 kHz even with the highest reflectivity mirror choices we have used in the models in the next section. For realistic choices of mirror reflectivities, if the length of the SRC is chosen such that the carrier frequency would resonate in it, we find GW sidebands within the spectrum of interest are also transmitted effectively. This mode of operation, with the length of the SRC chosen to resonate carrier frequency light, is conventionally known as *tuned* or *symmetrically tuned* mode. It is symmetric in the sense that sidebands spaced equally above and below the carrier frequency transmit equally. The technique allows us to build up the carrier field in the cavities, increasing the amplitude of our output signal, without destroying the sideband fields. The response is peaked at zero gravitational wave frequency but is relatively broadband, as we will see.

In the other mode, we attempt to adjust the phase of the reflectivity of the compound output coupler such that at least one sideband frequency is resonant in the arm cavities. Changing this reflectivity has no effect on the resonance of the carrier; for which only the PRC reflectivity is relevant. Again, because the SRC linewidth is broad enough to encompass the range of GW sidebands of interest, the phase of this reflectivity is relatively uniform over the spectrum of interest. In general it will exactly offset the excess phase (or the phase deficit) picked up in propagating through the arm cavity only for a sideband of a particular frequency. The linewidth of this resonance depends on the magnitude of the reflectivity associated with this phase, but also on the length of the arm cavities. Making the reflectivity of the SRC higher increases the sideband field at the resonant frequency and thus the sensitivity of the detector at that frequency, but due to the great length of the arm cavities, the result is that the detector bandwidth becomes narrower than

the spectrum of interest. This mode is conventionally known as *detuned* or *asymmetrically tuned* operation. Only sidebands created by a narrow range of GW frequencies, determined largely by the arm length we have chosen, are detectable in this mode. The amount of light falling on the detector is, however, higher in this narrowband mode, when the appropriate GW frequency is present, than it would be in the broadband mode for that same frequency.

Though this system offers better response in both modes than that depicted in figure 1, and eliminates many of the heating problems posed by that depicted in figure 2, it still forces us to choose between high sensitivity with low bandwidth, or high bandwidth with low sensitivity. The WLC proposal that will be described in section 4 would allow us to have at least the sensitivity of the narrowband mode over a spectrum as wide as that offered by broadband mode, so that a WLC-enhanced LIGO-type interferometer might offer the best of both worlds. In fact, we will show that the sensitivity can actually be much higher than that of the narrowband mode, while allowing a bandwidth as large as the broadband mode.

3. General model for Michelson-based GW detectors

The system depicted in figure 3 is also a more general case of those depicted in figures 1 and 2. If we model it mathematically and find its response, we may recover the response for the systems depicted in figures 1 and 2, or for a simple Michelson interferometer with no cavities, by setting the reflectivities of the appropriate mirrors equal to zero. In this section, we develop this general model.

Meers [21] first modeled this system in 1989, but his model is not given in a form that lends itself to the analysis of the effect of a WLC on the system. Furthermore, in the course of developing the model, he makes certain assumptions about mirror reflectivities and resonance conditions which render his final expression less than general. We will essentially follow his method in deriving the frequency response of the system illustrated in figure 3, but we will adopt a slightly different notation and avoid assuming any particular operating condition.

As Meers did, we will denote the reflectivity of the compound mirror M_{ICAR} by R_{IC} . This is not to be confused with the reflectivity of the mirror labeled M_C , which we will denote simply by R_C . We will denote the reflectivity of the compound mirror M_{ISB} by R_{IS} . Whereas he uses R_{IS} and R_{IC} to denote only the amplitude of the reflectivity, we will allow them to be complex numbers, giving information about both the amplitude and the phase of light reflected off the SRC and PRC, respectively. We can calculate these reflectivities from basic theory of a Fabry–Perot cavity, keeping in mind that they are frequency-dependent quantities wherever we use them.

The first step in the derivation is to quantify the effect of a GW on light. Let us choose our coordinates such that the effect of the GW on the metric of spacetime is described by [7]

$$ds^2 = dx^2(1 + h \cos \omega_g t) + dy^2(1 - h \cos \omega_g t) + dz^2 - c^2 dt^2. \quad (1)$$

Along the path of a light wave, $ds = 0$. Let us assume we have light propagating along the x axis. Then

$$dx^2(1 + h \cos \omega_g t) = c^2 dt^2 \Rightarrow \frac{dx}{dt} \approx c \left(1 - \frac{h}{2} \cos \omega_g t\right). \quad (2)$$

The phase the light accumulated as it travels is given by

$$\begin{aligned} \phi_x &= \int_{x_1}^{x_2} k dx = \int_{t-\tau}^t k \frac{dx}{dt} dt = \int_{t-\tau}^t kc \left(1 - \frac{h}{2} \cos \omega_g t\right) dt \\ &\Rightarrow \phi_x = \omega\tau - \frac{\omega h}{\omega_g} \sin\left(\frac{\omega_g \tau}{2}\right) \\ &\quad \times \left(\frac{e^{i\omega_g(t-\tau/2)} + e^{-i\omega_g(t-\tau/2)}}{2}\right). \end{aligned} \quad (3)$$

The calculation for a beam traveling along the y axis is identical, except that we use $\frac{dy}{dt} \approx c(1 + \frac{h}{2} \cos \omega_g t)$.

$$\Rightarrow \phi_y = \omega\tau + \frac{\omega h}{\omega_g} \sin\left(\frac{\omega_g \tau}{2}\right) \left(\frac{e^{i\omega_g(t-\tau/2)} + e^{-i\omega_g(t-\tau/2)}}{2}\right). \quad (4)$$

Of course $\omega\tau$ is the phase that the light would pick up in the absence of GWs. We define $\phi_{\text{prop}} = \omega\tau$ as the ordinary propagation phase. In our model, we assume that light traveling along one of the coordinate axes under the influence of GWs picks up a multiplication factor expressed as $e^{i\phi_x} = e^{i\phi_{\text{prop}}} e^{i\delta\phi_x} \cong e^{i\phi_{\text{prop}}} (1 + i\delta\phi_x)$ (where $\delta\phi_x = \phi_x - \phi_{\text{prop}}$) or as $e^{i\phi_y} \cong e^{i\phi_{\text{prop}}} (1 + i\delta\phi_y)$ (where $\delta\phi_y = \phi_y - \phi_{\text{prop}}$). By using these approximations, we are assuming that the modulation is small enough that the carrier power is effectively undepleted.

First we will consider the amplitude of the carrier field. Let us assume that a field with amplitude E_0 enters through $M_{1\text{CAR}}$, which has a transmittivity $T_{1\text{C}}$ and a reflectivity $R_{1\text{C}}$ at the carrier frequency. The field, after entering and reflecting off either arm-end mirror M_2 (which has a reflectivity R_2), returns to the PRC with an amplitude

$$E_1 = E_0 T_{1\text{C}} R_2 e^{-2ik_c L} \quad (5)$$

where L is the length of the arm-end cavity and k_c is the carrier wavenumber.

This field now reflects off $M_{1\text{CAR}}$, and then off M_2 again, returning to the PRC now with an amplitude

$$E_2 = E_0 T_{1\text{C}} R_2^2 R_{1\text{C}} e^{-4ik_c L}. \quad (6)$$

After each reflection thereafter the field picks up the same factor of $R_{1\text{C}} R_2 e^{-2ik_c L}$. The steady state field is the sum ($\sum_N E_N$) over all bounces. Therefore in steady state the carrier frequency field inside is

$$E'_{\text{car}} = E_0 T_{1\text{C}} R_2 e^{-2ik_c L} \sum_{N=1}^{\infty} (R_2 R_{1\text{C}} e^{-2ik_c L})^{N-1}. \quad (7)$$

Again, we have neglected the depletion of the carrier due to the modulation, in this model. Now the sideband fields being continually produced from this steady state carrier are given, under the approximation described above, by

$$\begin{aligned} E_{\text{SB}} &= E'_{\text{car}} e^{i\omega t} e^{i\phi_{\text{prop}}} (1 + i\beta(e^{i\omega_g(t-\tau/2)} + e^{-i\omega_g(t-\tau/2)})) \\ \text{where } \beta &= \frac{h\omega}{\omega_g} \sin(\omega_g \tau/2). \end{aligned} \quad (8)$$

The sidebands are reflected by the SRC in figures 3 and 4, and by the SRM in figure 2. Considering only the component at frequency $(\omega + \omega_g)$, we see that its initial amplitude is

$$E_{+1} = E'_{\text{car}} e^{i\omega t} e^{-2ik_c L} i\beta e^{i\omega_g(t-\tau/2)}. \quad (9)$$

Here we have used $\phi_{\text{prop}} = -2ik_c L$. This field reflects off the SRC and experiences a reflectivity $R_{1\text{S}}$. After another round trip the amplitude is

$$E_{+2} = E'_{\text{car}} e^{i\omega t} i\beta e^{i\omega_g(t-\tau/2)} R_{1\text{S}} R_2 e^{-2i\left(\frac{\omega+\omega_g}{c}\right)L_S} e^{-2ik_c L}. \quad (10)$$

Note that $(\omega + \omega_g)/c = k_+$, the wavenumber of the sideband. We have, in this expression, introduced another variable L_S , which is the length of the cavity in which the sidebands are propagating. In the case illustrated by figures 3 and 4, this L_S is the same as L , equal to the distance between the end test mass, M_2 , and the input test masses, M_{AB} . However, in the case illustrated by figure 2, these are two distinct numbers, with L_S being equal to the sum of the distance from the end test mass to the beamsplitter and that from the beamsplitter to the signal recycling mirror, and L being equal to the sum of the distance from the end test mass to the beamsplitter and that from the beamsplitter to the power recycling mirror. After n passes, then, the total field is

$$\begin{aligned} E'_+ &= \left(\sum_n E_{+n}\right) = E'_{\text{car}} e^{i\omega t} i\beta e^{i\omega_g(t-\tau/2)} e^{-2ik_c L} \\ &\quad \times \sum_{n=1}^{\infty} R_{1\text{S}}^{n-1} R_2^{n-1} e^{-2i(n-1)(\omega+\omega_g)L_S/c}. \end{aligned} \quad (11)$$

Doing the geometric series sums for E'_{car} and E'_+ , we find that the output field transmitted through the SRC, $E_+ = E'_+ T_{1\text{S}}$, is given by

$$\begin{aligned} \frac{E_+}{E_0 e^{i\omega t}} &= \frac{T_{1\text{S}} T_{1\text{C}} R_2}{1 - R_2 R_{1\text{C}} e^{-2ik_c L}} \\ &\quad \times \frac{i(h\omega/\omega_g) \sin(\omega_g \tau/2) e^{-2ik_c L} e^{i\omega_g(t-\tau/2)} e^{-2ik_c L}}{1 - R_{1\text{S}} R_2 e^{-2i(\omega+\omega_g)L_S/c}} \end{aligned} \quad (12)$$

The notation here is slightly different from that used by Meers [21], but the result agrees with his provided we define $2L/c = \tau$, $\delta_C = (-2\omega L/c) \bmod 2\pi$ and $\delta_S = (-2\omega L_S/c) \bmod 2\pi$. By leaving the expression in terms of the separate wavenumbers of the sidebands and carrier, however, we leave ourselves the option of easily including dispersive effects in this calculation at the next stage.

For the minus-sideband, the expression is the same, except with $\omega_g \rightarrow -\omega_g$, and with $R_{1\text{S}}$ potentially taking on a different value, since it is a frequency-dependent reflectivity. These amplitudes do not tell us the frequency response of our device directly, however. In practice, the sidebands are detected by allowing a small amount of carrier frequency light to leak through and detecting the beat signal. To find the total response of the interferometer we need to calculate the amplitude of that beat signal:

$$\delta I = E_L E_+^* + E_+ E_L^* + E_L E_-^* + E_- E_L^*. \quad (13)$$

Here E_L is the carrier frequency field with which we are mixing our sidebands:

$$E_L = (A/E_0) e^{i(\omega t + \phi)}. \quad (14)$$

In order to do this sum, it is convenient to change our notation slightly. Let $R_{1C} = r_{1C}e^{i\phi_{r1C}}$, and let $R_{1S_+} = r_{1S_+}e^{i\phi_{r1S_+}}$ be the reflectivity of the SRC at the plus-sideband frequency, while $R_{1S_-} = r_{1S_-}e^{i\phi_{r1S_-}}$ is the reflectivity of the SRC at the minus-sideband frequency. In general, lower case letters for the reflectivity or transmittivity will now be used to denote the magnitude only. We also choose to insert a couple of multiplicative factors equal to one, marked with square brackets. With this convention the equation above may be rewritten as

$$\frac{E_+}{E_0 e^{i\omega t}} = \frac{t_{1S_+} e^{i\phi_{r1S_+}} t_{1C} e^{i\phi_{r1C}} r_2 i \hbar \omega \sin(\omega_g \tau / 2) e^{i\omega_g(t-\tau/2)}}{\omega_g} \times \frac{e^{-2ik_c L} [e^{i\phi_{r1C}} e^{-i\phi_{r1C}}]}{(1 - r_2 r_{1C} e^{i\phi_{r1C}} e^{-2ik_c L})} \times \frac{e^{-2ik_c L} [e^{i\phi_{r1S_+}} e^{-i\phi_{r1S_+}}] [e^{-2ik_+ L_S} e^{2ik_+ L_S}]}{(1 - r_2 r_{1S_+} e^{i\phi_{r1S_+}} e^{-2ik_+ L_S/c})}. \quad (15)$$

These additional factors allow us to make use of the identity $\frac{e^{i\phi}}{1 - \rho_1 \rho_2 e^{i\phi}} = \frac{e^{i\phi} - \rho_1 \rho_2}{(1 - \rho_1 \rho_2)^2 (1 + F' \sin^2(\phi/2))}$, where $F' = \frac{4\rho_1 \rho_2}{(1 - \rho_1 \rho_2)^2}$, to write the output in terms of a cavity finesse. We will use F'_C for the finesse of the cavity as experienced by the carrier frequency light, F'_{S_+} for the plus-sideband and F'_{S_-} for the minus-sideband.

We now have

$$\frac{E_+}{E_0 e^{i\omega t}} = \frac{t_{1S_+} t_{1C} r_2 i \hbar \omega \sin(\omega_g \tau / 2)}{\omega_g} \times \left(\frac{e^{-2ik_c L + i\phi_{r1C}} - r_2 r_{1C}}{(1 - r_2 r_{1C})^2 \left(1 + F'_C \sin^2\left(\frac{-2k_c L + \phi_{r1C}}{2}\right)\right)} \right) \times \left(\frac{e^{-2ik_+ L + i\phi_{r1S_+}} - r_2 r_{1S_+}}{(1 - r_2 r_{1S_+})^2 \left(1 + F'_{S_+} \sin^2\left(\frac{-2k_+ L_S + \phi_{r1S_+}}{2}\right)\right)} \right) \times e^{i\omega_g(t-\tau/2)} e^{i\phi_{r1S_+}} e^{i\phi_{r1C}} e^{-i\phi_{r1C}} e^{-2ik_c L} e^{-i\phi_{r1S_+}} e^{2ik_+ L_S}. \quad (16)$$

We would like to separate out the part of this expression that represents the sideband resonance in the arms. To this end, we define

$$\xi_{\pm} = \frac{t_{1C} t_{1S_{\pm}} r_2 i \hbar \omega \sin(\omega_g \tau / 2)}{\omega_g (1 - r_2 r_{1C})^2 (1 - r_2 r_{1S_{\pm}})^2}. \quad (17)$$

This contains all of the scaling information which is independent of the length of the arms. Also we let

$$B e^{i\phi_B} = \frac{e^{-2ik_c L + i\phi_{r1C}} - r_2 r_{1C}}{1 + F'_C \sin^2(k_c L - \phi_{r1C}/2)}. \quad (18)$$

Now B and ϕ_B carry the information about the magnitude and phase of the carrier field in the arm cavities. With this notation

$$\frac{E_+}{E_0 e^{i\omega t}} = i \xi_+ B \left(\frac{1 - r_2 r_{1S_+} e^{2ik_+ L - i\phi_{r1S_+}}}{1 + F'_{S_+} \sin^2(k_+ L_S - \phi_{r1S_+}/2)} \right) e^{i\omega_g(t-\tau/2)} \times e^{i\phi_{\text{eff}}} e^{i\phi_{r1S_+}} e^{i\phi_B} \quad (19)$$

where $\phi_{\text{eff}} = \phi_{r1C} - \phi_{r1C} - 2ik_c L$.

With this expression and some trigonometric identities, it is now relatively straightforward to calculate the total response of our device. In keeping track of the phase of the carrier,

it proves convenient to define $\phi_{\text{net}} = (\phi_{\text{eff}} - \phi + \phi_B)$. We also replace τ with $2L/c$ at this point so as to make all length dependences explicit.

We find that

$$E_+ E_L^* + E_+^* E_L = \frac{-2AB\xi_+}{1 + F'_{S_+} \sin^2(k_+ L_S - \phi_{r1S_+}/2)} \times \left[\sin\left(\omega_g\left(t - \frac{L}{c}\right) + \phi_{r1S_+} + \phi_{\text{net}}\right) - r_2 r_{1S_+} \right] \times \sin\left(\omega_g\left(t - \frac{L}{c}\right) + \phi_{r1S_+} + \phi_{\text{net}} + 2k_+ L_S - \phi_{r1S_+}\right). \quad (20)$$

Finally, we choose

$$\phi_C = \phi_{\text{net}} - \pi/2 = \phi_{r1C} - \phi_{r1C} - 2k_c L - \phi + \phi_B - \pi/2. \quad (21)$$

This variable keeps track of the total phase of the carrier, and the term $\pi/2$ allows us to turn our sine functions into cosine functions. Note that the unsubscripted ϕ comes from assuming our sidebands are beating with a carrier frequency field of the form $E_L = (A/E_0)e^{i(\omega t + \phi)}$. We will assume that this phase is controllable, and that we can always choose it so that the output is optimum. The signal from our device is then

$$\begin{aligned} \delta I &= E_L E_+^* + E_+ E_L^* + E_L E_-^* + E_- E_L^* \\ &= 2AB \left[\left(\frac{\xi_+ \cos(\omega_g(t - L/c))}{1 + F'_{S_+} \sin^2(k_+ L_S - \phi_{r1S_+}/2)} \right) \times (r_2 r_{1S_+} \cos(2k_+ L - \phi_{r1S_+} + \phi_{r1S_+} + \phi_C) - \cos(t_{1S_+} + \phi_C)) + \left(\frac{\xi_+ \sin(\omega_g(t - L/c))}{1 + F'_{S_+} \sin^2(k_+ L_S - \phi_{r1S_+}/2)} \right) \times (-r_2 r_{1S_+} \sin(2k_+ L - \phi_{r1S_+} + \phi_{r1S_+} + \phi_C) + \sin(t_{1S_+} + \phi_C)) + \left(\frac{\xi_- \cos(\omega_g(t - L/c))}{1 + F'_{S_-} \sin^2(k_- L_S - \phi_{r1S_-}/2)} \right) \times (r_2 r_{1S_-} \cos(2k_- L - \phi_{r1S_-} + \phi_{r1S_-} + \phi_C) - \cos(t_{1S_-} - \phi_C)) + \left(\frac{\xi_- \sin(\omega_g(t - L/c))}{1 + F'_{S_-} \sin^2(k_- L_S - \phi_{r1S_-}/2)} \right) \times (r_2 r_{1S_-} \sin(2k_- L - \phi_{r1S_-} + \phi_{r1S_-} + \phi_C) - \sin(t_{1S_-} + \phi_C)) \right] \equiv P \cos(\omega_g(t - L/c)) + Q \sin(\omega_g(t - L/c)). \quad (22) \end{aligned}$$

To find the magnitude of this signal, then, we have only to add the amplitudes of the sine and cosine terms in quadrature:

$$|\delta I| = \sqrt{P^2 + Q^2}. \quad (23)$$

This rather complicated expression gives the full response of the system illustrated in figure 3, if we set $L_S = L$. In the limit where $r_{1S_+} = r_{1S_-} = r_{1C}$, this also gives the response of the simpler system illustrated in figure 1. Finally, this expression can give us the response of the system illustrated in figure 2 as well, where $L_S \neq L$, $r_{1S_{\pm}}$ is equal to the reflectivity of the SRM, and r_{1C} is equal to that of the PRM.

A GW detector, in the configuration illustrated in figure 3 and described by the above equation, has two basic modes of operation, as described in section 2. In figure 5, the response

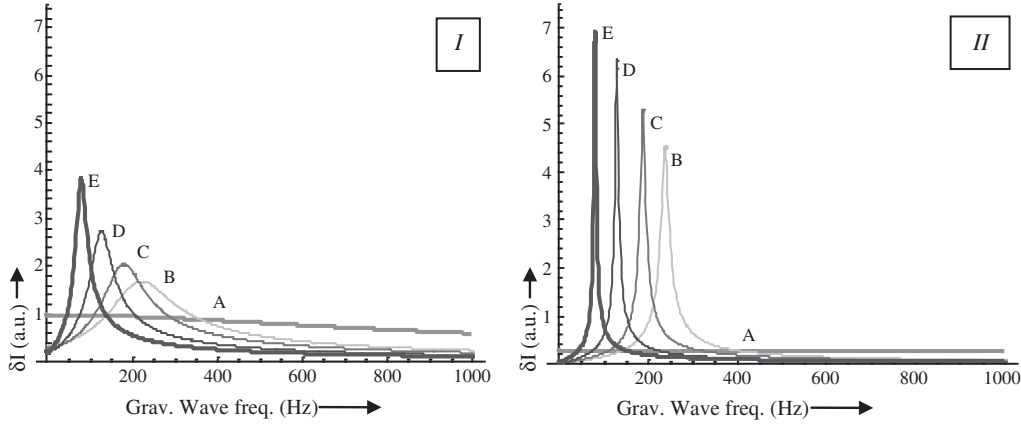


Figure 5. (I) Output signal as a function of gravitational frequency for a GW detector of the type illustrated in figure 3, using the advanced LIGO parameters of [16], under different operating conditions. The tuned mode response is normalized to one at zero frequency. (II) The same but with the signal recycling mirror transmissivity decreased from 0.2 to 0.02. For both graphs, the detunings, expressed in terms of phase shifts, are given: (A) 0° (tuned mode), (B) 20° , (C) 25.2° , (D) 36° and (E) 54° .

Table 1. Values used in plotting figure 5, taken from [20].

$r_2 = 0.9999$;	$r_{AB} = \sqrt{1 - 0.014}$;
$k_c = 2 * \pi / ((1064 * 10^{(-9)}))$;	$t_{AB} = \sqrt{0.014}$;
$c = 3 * 10^8$;	$a = 0.991$;
$w = k_c * c$;	$m = 5.420675 * 10^7$;
$h = 10^{(-12)}$;	$L_{prc} = 2\pi m / k_c$
$A = 1/25.65$;	$\phi_c = \phi_{r_{1s}} + f_g = 0$
$r_D = \sqrt{1 - 0.03}$;	$n = 3.75446 * 10^9$;
$t_D = \sqrt{0.03}$;	$L = (2\pi n + \phi_{r_{1c}}/2) / k_c$
$r_C = \sqrt{1 - 0.2}$;	$L_{srcSymMD0} = (2 * \pi * (10.53157 * 10^7) + \pi) / (2 * k_c)$
$t_C = \sqrt{0.2}$;	

for the two cases, calculated using the equation above, is plotted. These graphs are to be compared with those shown in [19] for a similar system with different reflectivity and length parameters. We display the response both with the currently planned advanced LIGO value for the SRM reflectivity r_C and with a higher reflectivity, to illustrate the effect on the signal response. The higher reflectivity allows much larger signal responses but with much narrower bandwidths.

The values presented in table 1 were used in calculating the response.

Both h , the amplitude of the GW, and A , the amplitude of the homodyning beam, are simple scale factors in these equations, appearing only as multiplicative constants. Their values are arbitrarily adjusted to normalize the response to one for the tuned case at zero GW frequency. The lower case ‘a’ is the factor by which the field is assumed to be reduced on each pass through the SRC due to losses, and multiplies the reflectivity of the SRM in the Fabry–Perot calculations of the SRC reflectivity, i.e. $r_c \rightarrow a * r_c$. The variables r_2 , r_{AB} , t_{AB} , r_C , t_C , r_D and t_D represent the reflectivity and transmittivity of the mirrors labeled M_2 , M_{AB} , M_C and M_D , respectively, in figures 3 and 4. These values are taken from [17], and are the currently planned values for the advanced LIGO system.

$L_{srcSymMD0}$ represents the symmetrically tuned (‘mode 0’) length of the SRC. The reflectivity of the SRC is calculated from standard Fabry–Perot theory starting from this value for

the length of the cavity, with a variable detuning. In these calculations, the fact that one of the cavity mirrors has its substrate facing inwards must be taken into account. This alters the phase of the reflectivity of that mirror by 180° , and thus alters the resonant length. The same is true of the PRC. Again, the SRC need not be 100% transmitting and is not, even on resonance, due to the mismatch in r_{AB} and r_C . The more reflective the SRC is, the higher the signal will be, so long as the reflectivity of SRC is still small enough to allow the relevant sideband spectrum to fit within the bandwidth of the arms. The transmittivity of the SRC, though not unity, is nevertheless maximized for the chosen mirror reflectivities in these tuned mode plots. The reflectivity is higher, and the transmittivity lower, in detuned mode, but the magnitude cannot be chosen independently of the phase. This reflection phase could run between zero and 2π if the mirrors r_{AB} and r_C were matched, but this would mean lowering the reflectivity to zero in tuned mode, which would not be ideal. The attempt to resonate higher frequency sidebands in detuned mode therefore comes at the expense of the signal in tuned mode operation, and the mirror reflectivities r_{AB} and r_C are chosen with this trade-off in mind.

Clearly hybrid modes of operation exist, with different choices for the lengths of the SRC and PRC and different choices for the phase of the carrier frequency beam with which the sidebands beat, but these two cases are enough to give a general idea of the behavior in the broadband tuned mode

versus narrowband detuned mode using the advanced LIGO parameters.

4. Dispersive effects

Having written the output of the device in terms of the sideband wavenumbers k_+ and k_- , we are now in a position to include easily the effects of dispersion on the system. The effect of the medium is to change the wavelength of light within it, so that $\lambda_{\text{medium}} = \lambda_{\text{vacuum}}/n$, where n is the index of refraction of the medium. Equivalently, we may multiply the wavenumber by n , i.e. $k_{\text{medium}} = nk_{\text{vacuum}}$.

If we had a Fabry–Perot cavity of length L , the propagation phase light would ordinarily pick up on traveling from one end to the other is

$$\theta_{\text{vacuum}} = kL \quad (\text{where } k = k_{\text{vacuum}}). \quad (24)$$

If, however, we assume a cavity of length L partially filled by a medium of length l , that phase becomes

$$\theta = k(L - l) + n(\omega)kl. \quad (25)$$

The phase picked up by light making one round trip in the cavity is then

$$\theta_{\text{r.t.}} = 2k(L - l) + 2n(\omega)kl. \quad (26)$$

Assuming the light does not pick up any additional phase shifts as it propagates, the resonance condition is

$$\theta_{\text{r.t.}} = 2\pi m \quad (\text{for integer } m). \quad (27)$$

If the light does pick up some phase shift, e.g. by reflecting off a phase-shifting mirror, then the resonance condition is altered so that the total phase picked up is equal to $2\pi m$, and the round trip propagation phase is equal to $2\pi m$ minus the extra phase due to the reflection.

In either case, resonance requires that the round trip phase $\theta_{\text{r.t.}}$ be equal to some predetermined constant. In free space, there would be only one value of ω which would fulfill the resonance condition. In a medium, however, we may have $\theta_{\text{r.t.}}$ depend on ω in a nonlinear way. If we require that

$$\left. \frac{d\theta_{\text{r.t.}}}{d\omega} \right|_{\omega_0} = 0 \quad (28)$$

at some frequency ω_0 , then the round trip phase will not change with frequency at all for very small deviations from ω_0 , and will change by very small amounts for some range of frequencies around ω_0 . If ω_0 happens to be the resonant frequency of the cavity, then a range of frequencies around ω_0 will also be very close to resonance. The key to making a WLC is to make this range sufficiently large that the cavity resonates over a much wider bandwidth than it would if it were empty.

Substituting $k = \omega/c$ into equation (26) (since k here is the vacuum wavenumber), and taking the derivative, we find

$$\begin{aligned} \left. \frac{d\theta_{\text{r.t.}}}{d\omega} \right|_{\omega_0} &= \left[\frac{d}{d\omega} \left(2\frac{\omega}{c}(L - l) + 2n(\omega)\frac{\omega}{c}l \right) \right]_{\omega_0} \\ &\approx 2 \left(\frac{L}{c} + \left. \frac{dn}{d\omega} \right|_{\omega_0} \frac{\omega_0}{c} l \right) \quad (\text{if } n(\omega_0) \approx 1). \end{aligned} \quad (29)$$

Therefore the condition $\left. \frac{d\theta_{\text{r.t.}}}{d\omega} \right|_{\omega_0} = 0$ requires that

$$\left. \frac{dn}{d\omega} \right|_{\omega_0} = -\frac{L}{l} \frac{1}{\omega_0}. \quad (30)$$

The simplest model for a WLC assumes an index of refraction which is linear in ω and has a slope given by the equation above:

$$n(\omega) = 1 + \frac{-L}{l} \frac{1}{\omega_0} (\omega - \omega_0). \quad (31)$$

More complete models might assume $n(\omega)$ has the lineshape of the derivative of a Lorentzian, and choose the coefficients in the equation for this lineshape to give the appropriate slope at the center, or even more realistically, reproduce the lineshape of an index due to double gain peaks [2], for example, again with coefficients chosen such that the index has the appropriate slope between the two peaks.

Whichever functional form of $n(\omega)$ we choose, we may plug it into equation (25) to find its effect on the phase of light propagating through the cavity. The linear form of $n(\omega)$, for instance, gives

$$\begin{aligned} \theta &= k(L - l) + \frac{-L}{l} \frac{1}{\omega_0} (\omega - \omega_0)(kl) \\ &= k(L - l) + \frac{-L}{k_0} (k - k_0)(k) \end{aligned} \quad (32)$$

where $k_0 = \omega_0/c$ and k is the vacuum wavenumber. All standard Fabry–Perot cavity analysis still applies, provided we use this expression for the propagation phase of light traveling from one end to the other of the cavity.

In general, in order to find the effect of changing the arm cavities into WLCs, on a LIGO-type GW detector, we can make the following substitutions:

$$\begin{aligned} k_+L_S &\rightarrow k_+(L_S - l) + n(k_+)k_+l \\ k_-L_S &\rightarrow k_-(L_S - l) + n(k_-)k_-l \\ k_cL_S &\rightarrow k_c(L_S - l) + n(k_-)k_-l \end{aligned} \quad (33)$$

where $n(k)$ has the appropriate slope at the resonant frequency. Note that these expressions imply that we are placing the medium in the cavity of length L_S . In the type of system illustrated in figure 3, where $L_S = L$, this means the medium must be placed in the arms of the interferometer. In the case illustrated by figure 2, however, the medium may be placed between the beamsplitter and the signal recycling mirror. In any case, we want to place it in whatever cavity stores the sidebands and has a length of the order of 4 km, in order to broaden the ordinarily very narrow linewidth associated with such a long resonator. Later in this section, we show a modified version of the configuration in figure 3 where the WLC effect can be realized by placing the medium between the SRM and an auxiliary mirror.

In the expressions above, we have used the linear form of $n(\omega)$, without indicating a turn around point for the index function. Using more realistic functional forms of $n(\omega)$ gives a more realistic analysis of the behavior of the system. In figure 6, we plot the effects on the output of the interferometer using a slightly more complex model for the index, which

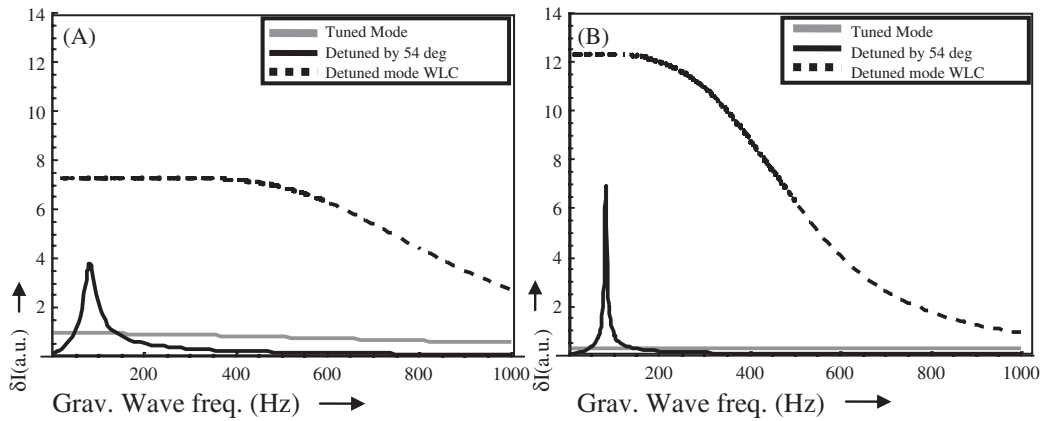


Figure 6. (A) Tuned mode response, detuned mode response, and detuned mode response with WLC for a cavity/interferometer with advanced LIGO reflectivities and lengths. (B) The same, but using an SRM with a transmissivity of $t_c^2 = 0.02$ instead of $t_c^2 = 0.2$ as in advanced LIGO. In both graphs the dispersive material is chosen to have $dn/d\omega = -L/(\omega_0 l)$ over a linewidth of approximately 1600 Hz centered around that resonant frequency, but the output begins to fall when the other sideband is no longer within the linear region.

assumes its lineshape is that of the derivative of a Lorentzian with a linewidth of approximately 16 kHz, with the scaling of the Lorentzian function chosen to give an appropriate slope to the index function at the center. The bandwidth will, in practice, depend on the specific choice of dispersive material. In our experimental demonstrations of the WLC [10], we have seen a linear bandwidth of approximately 5 MHz which is considerably broader than the GW bandwidth of interest. For these simulations, however, we have chosen to assume a narrower linewidth in order to show clearly the effect of the material on gravitational sideband frequencies near or outside that linear bandwidth. For convenience we have chosen $l = L$ for these plots.

In general a WLC produces the same peak response as an empty cavity, but with a broader bandwidth. However, in figure 6, the peak WLC response is twice as large as the peak of the detuned mode response. This is because in the WLC gravitational wave detector, both GW sidebands resonate instead of just one.

These graphs illustrate that the WLC-based GW detector is not just broader in bandwidth than the currently planned advanced LIGO model, but potentially more sensitive as well, since the mirror reflectivities could be optimized for sensitivity in narrowband mode rather than for bandwidth.

The cases illustrated above are for the advance LIGO-type detector illustrated in figure 3. We have also carried out the derivation, and developed the frequency response graph, for the type of detector illustrated in figure 2, with and without a WLC. This system is similar to that for which we have already plotted the output, except that the finesse of the arm cavities for the SBs cannot be dynamically controlled—it is given by the reflectivity of the SRM and does not vary with its position. Nevertheless, the behavior in detuned mode is very similar. Incorporating a WLC again gives a broadband response equal to twice the peak value of the narrowband response, since with the WLC, both sidebands will resonate along with the carrier. This is illustrated in figure 7. In this case, it is worth noting that again, increasing the reflectivity of the SRM increases the sensitivity of the detector without

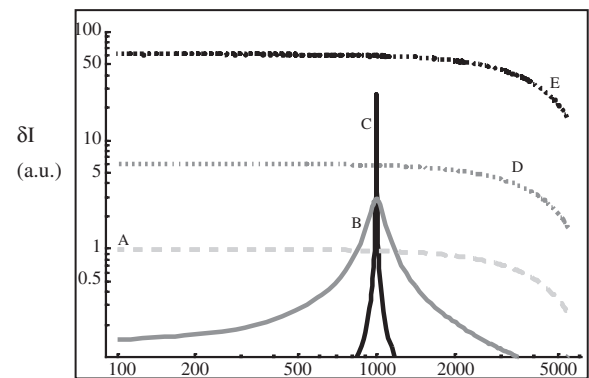


Figure 7. Illustration of the effect of WLC on the configuration shown in figure 2: (A) $r_{\text{SRM}} = 0$, (B) detuned mode, $r_{\text{SRM}} = \sqrt{1 - 0.1}$, (C) detuned mode, $r_{\text{SRM}} = \sqrt{1 - 0.001}$, (D) same as (B) but with WLC and (E) same as (C) but with WLC.

compromising the bandwidth, so that with the incorporation of a WLC, a detector of this type can be made far more sensitive, for a given carrier power, than would be feasible without the WLC.

As discussed in [8], this simpler type of design may in fact be more suitable for use with a WLC than the design illustrated by figure 3. In this configuration, illustrated by figure 2, the dispersive medium may be placed outside the interferometer arms, between the beamsplitter and the signal recycling mirror. In this case, the beam power within the medium can be smaller, since the high power carrier is not incident on the medium in this configuration. The design illustrated by figure 2 also requires a simpler control system, with fewer cavities to lock. It does suffer from the issues regarding the heating of the beamsplitter as described earlier, and is slightly less flexible.

The two WLC-enabled designs considered above each suffers from a significant practical constraint. In the first case, the WLC element is added inside the arm cavities of figure 3. Since this requires two separate WLC elements to be inserted in the two arms, it would be difficult to match dispersion exactly. Furthermore, since the beams inside the arm cavities

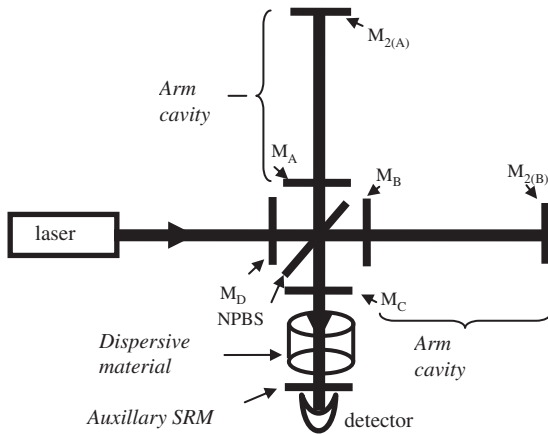


Figure 8. Dual recycling system with auxiliary signal recycling mirror, which allows for large carrier build up in arms, low power on primary beamsplitter, and, if the reflectivity of M_C is matched to that of M_{AB} , for high finesse signal recycling over broad band using WLC.

are very large in diameter, the WLC elements have to be very large as well. The best WLC medium we have identified for the wavelength used in the LIGO apparatus is a photorefractive crystal [3]. It would be very difficult to make such a crystal big enough to meet this requirement. Finally, the presence of the very strong pump beams would most likely cause heating problems in the WLC medium. In the second design, the WLC element is placed between the beamsplitter and the SRM of the configuration shown in figure 2. However, the configuration of figure 2 has already been discounted in the LIGO as well as the AdLIGO design because of the problem of heating the beamsplitter.

In figure 8, we offer a new WLC-enabled design that circumvents all these practical constraints. In this design M_{AB} and M_C have matched reflectivities. If the distance between them is such that the carrier is resonant, and the linewidth broad enough that the relevant range of sidebands resonate as well, these two mirrors effectively disappear for signal recycling. The cavity they form is transparent to the sideband light and causes no effective phase shift. The sidebands then encounter the auxiliary mirror, in front of the detector, and are reflected back through the transparent cavity again into the arms. This system is, as far as the sidebands are concerned, the same as that modeled in figure 2. However, it allows the power in the arms to be kept high while keeping the power on the beamsplitter low. Finally, it allows us to place the dispersive medium outside the interferometer arms, between the two mirrors which lie between the beamsplitter and the detector. The design proposed in figure 8 can be implemented in a non-invasive manner by a minor modification of the current AdLIGO design. The beam size before the auxiliary mirror and after the SRM can be reduced using lenses in order to accommodate the size of a photorefractive crystal.

We simulated this situation with $r_C = r_{AB} = \sqrt{1 - 0.014}$ for two different values of the auxiliary mirror reflectivity. The distance between M_{AB} and M_C was reduced to 0.5 m, while the distance between M_C and the auxiliary mirror was chosen

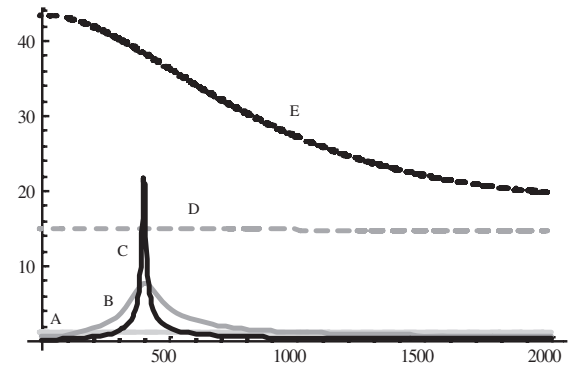


Figure 9. Response functions for the system depicted in figure 8. (A) $r_{AUX} = 0$, no dispersive material, (B) $r_{AUX} = \sqrt{1 - 0.02}$, no dispersive material, (C) $r_{AUX} = \sqrt{1 - 0.002}$, no dispersive material, (D) same as (B) but including material with critically anomalous dispersion at the location shown in figure 8 and (E) same as (C) but including material with critically anomalous dispersion at the location shown in figure 8.

to be ~ 0.57 m. The results, with and without the anomalously dispersive material, are shown in figure 9.

5. Conclusion

Almost all Michelson-based GW detectors can be described by equation (22) of this paper. This equation follows from basic Fabry–Perot theory, provided the arms of the interferometer are identical, and involves treating some pairs of mirrors as a single compound mirror with a frequency-dependent reflectivity, in certain cases.

The effect of introducing a medium into such a system is to change the propagation phase of the light within the long arm cavities. If the medium has a negative dispersion with a slope given by equation (30), that propagation phase will not vary with frequency over some range, and the resonance bandwidth of the cavity will be broadened. This will have the effect, for all of the variations on the Michelson interferometer that we have discussed, of both broadening the bandwidth of the detector and increasing its sensitivity to some degree by preventing destructive interference within the cavity.

The method given here for calculating the effect of a WLC on any Michelson-based GW detector allows us to consider a variety of different designs, each with its own advantages and disadvantages. The graph shown in figure 9 shows that a WLC could significantly improve a GW detector, with enhanced sensitivity as well as bandwidth, building on the design currently proposed for advanced LIGO.

Acknowledgments

This work was supported by DARPA through the slow light program under grant FA9550-07-C-0030, by AFOSR under grant FA9550-06-1-0466, and by the NSF IGERT program under grant DGE-080-1685.

References

- [1] Hough J, Meers B J, Newton G P, Robertson N A, Ward H, Schutz B F, Corbett I F and Drever R W P 1987 Gravitational wave astronomy—potential and possible realisation *Vistas Astronom.* **30** 109
- [2] Pati G S, Salit M, Salit K and Shahriar M S 2007 Demonstration of a tunable-bandwidth white-light interferometer using anomalous dispersion in atomic vapor *Phys. Rev. Lett.* **99** 133601
- [3] Yum H N, Salit M, Pati G S, Tseng S, Hemmer P R and Shahriar M S 2008 Fast-light in a photorefractive crystal for gravitational wave detection *Opt. Express* **16** 20448–56
- [4] Sun Q, Shahriar M S and Zubairy M S 2007 Slow light and fast light in a photorefractive crystal <http://lapt.eecs.northwestern.edu/preprints/slow-fast-prc.pdf>
- [5] Cooperstock F I and Faraoni V 1993 Laser-interferometric detectors of gravitational waves *Class. Quantum Grav.* **10** 1189
- [6] Black E D and Gutenkunst R N 2003 An introduction to signal extraction in interferometric gravitational wave detectors *Am. J. Phys.* **71** 365
- [7] Hartle J B 2003 *Gravity: An Introduction to Einstein's General Relativity* (San Francisco, CA: Addison-Wesley)
- [8] Shahriar M S and Salit M 2008 Application of fast light in gravitational wave detection with interferometers and resonators *J. Mod. Opt.* **55** 3133–47
- [9] Rinkleff R H and Wicht A 2005 The concept of white light cavities using atomic phase coherence *Phys. Scr.* **T118** 85
- [10] Wicht A, Rinkleff R-H, Spani Molella L and Danzmann K 2002 Comparative study of anomalous dispersive transparent media *Phys. Rev. A* **66** 063815
- [11] Rocco A, Wicht A, Rinkleff R-H and Danzmann K 2002 Anomalous dispersion of transparent atomic two- and three-level ensembles *Phys. Rev. A* **66** 053804
- [12] Wicht A, Muller M, Rinkleff R-H, Rocco A and Danzmann K 2000 Experimental demonstration of negative dispersion without absorption *Opt. Commun.* **179** 107–15
- [13] Wicht A, Danzmann K, Fleischhauer M, Scully M, Miiller G and Rinkleff R-H 1997 White-light cavities, atomic phase coherence and gravitational wave detectors *Opt. Commun.* **134** 431–9
- [14] Salit M, Pati G S, Salit K and Shahriar M S 2007 Fast-light for astrophysics: super-sensitive gyroscopes and gravitational wave detectors *J. Mod. Opt.* **54** 2425
- [15] Wise S, Mueller G, Reitze D, Tanner D B and Whiting B F 2004 Linewidth-broadened Fabry–Perot cavities within future gravitational wave detectors *Class. Quantum Grav.* **21** S1031
- [16] Wise S *et al* 2005 Phase effects in the diffraction of light: beyond the grating equation *Phys. Rev. Lett.* **95** 013901
- [17] LIGO Laboratory/LIGO Scientific Collaboration 2007 Advanced LIGO reference design: LIGO-060056-08-M <http://www.ligo.caltech.edu/docs/M/M060056-08/M060056-08.pdf>
- [18] Strain K A *et al* 2003 Sensing and control in dual-recycling laser interferometer gravitational-wave detectors *Appl. Opt.* **42** 1244
- [19] Mizuno J, Strain K A, Nelson P G, Chen J M, Schilling R, Rudiger A, Winkler W and Danzmann K 1993 Resonant sideband extraction: a new configuration for interferometric gravitational wave detectors *Phys. Lett. A* **175** 273–6
- [20] LIGO Laboratory/LIGO Scientific Collaboration 2008 AdvLIGO interferometer sensing and control conceptual design: LIGO-T070247-01-I <http://www.ligo.caltech.edu/docs/T/T070247-01.pdf>
- [21] Meers B J 1989 The frequency response of interferometric gravitational wave detectors *Phys. Lett. A* **142** 465